nature Vol 465|27 May 2010|doi:10.1038/nature09049

LETTERS

Onset and migration of spiral troughs on Mars revealed by orbital radar

Isaac B. Smith[1] & John W. Holt[1]

The landscape of the north polar layered deposits of Mars (NPLD) is dominated by a pinwheel array of enigmatic spiral troughs[1]. The troughs have intrigued planetary scientists since the Mariner 9 spacecraft returned the first close-up image in 1972, but conclusive evidence of their origin has remained elusive. Debate continues regarding all aspects of the troughs, including the possibility that they have migrated[2–5], their age in relation to the current NPLD surface[6], and whether they are fundamentally erosional[6,7] or constructional[2,4] features. The troughs are probably related to climatic processes[2,8], yet the nature of this relationship has remained a mystery. Previous data characterizing only the exposed NLPD surface were insufficient to test these hypotheses. Here we show that the central spiral troughs initiated after deposition of three-quarters of the NPLD, quickly reached a stable morphology and migrated approximately 65 kilometres poleward and 600 metres in altitude over the past two million years or so. Our radar stratigraphy rules out hypotheses of erosional incision post-dating deposition[6,7,9,10], and instead largely validates an early hypothesis for constructional trough migration[2–5] with wind transport and atmospheric deposition as dominant processes. These results provide hard constraints for palaeo-climate models and a new context for evaluating imagery, spectral data, and now radar sounding data, the better to understand the link between orbital parameters and climate, the role of climate in shaping the polar ice of Mars, and eventually, the age of the polar deposits themselves[8,11–13].

The spiral troughs of the NPLD (Fig. 1a) were found in Mariner and Viking imagery to have layers exposed on their equator-facing (northern) slopes, whereas their pole-facing (southern) slopes showed no such layers[3,14,15]. This observation implied erosion on the equator-facing slope and deposition on the pole-facing slope, leading to a hypothesis of northward scarp migration[3]. The process proposed[2,4] to explain such migration involves uniform deposition over the region accompanied by preferential erosion of the equator-facing slope due to solar ablation, along with wind transport of eroded material to the pole-facing slope by katabatic winds.

In contrast to this constructional migration scenario, a number of other hypotheses have been proposed that support spiral trough formation only after NPLD deposition. Such mechanisms include random erosion organizing into large-scale spirals[9], differential rotation between the inner and outer deposits[16], albedo contrasts from wind-deposited dust[17], along-trough wind erosion[6,14], accublation derived from upward flow beneath the troughs[18], and Coriolis-deflected glacial surges[19,20]. The wide range of ideas put forth in the past three decades regarding these major features emphasizes how limited is our knowledge of fundamental processes governing polar ice on Mars.

Although they are essential to our current understanding of stratigraphy in the polar layered deposits, optical techniques allow only the interpretation of layers that have been exposed by erosion. Radar has been instrumental in mapping subsurface stratigraphy within ice

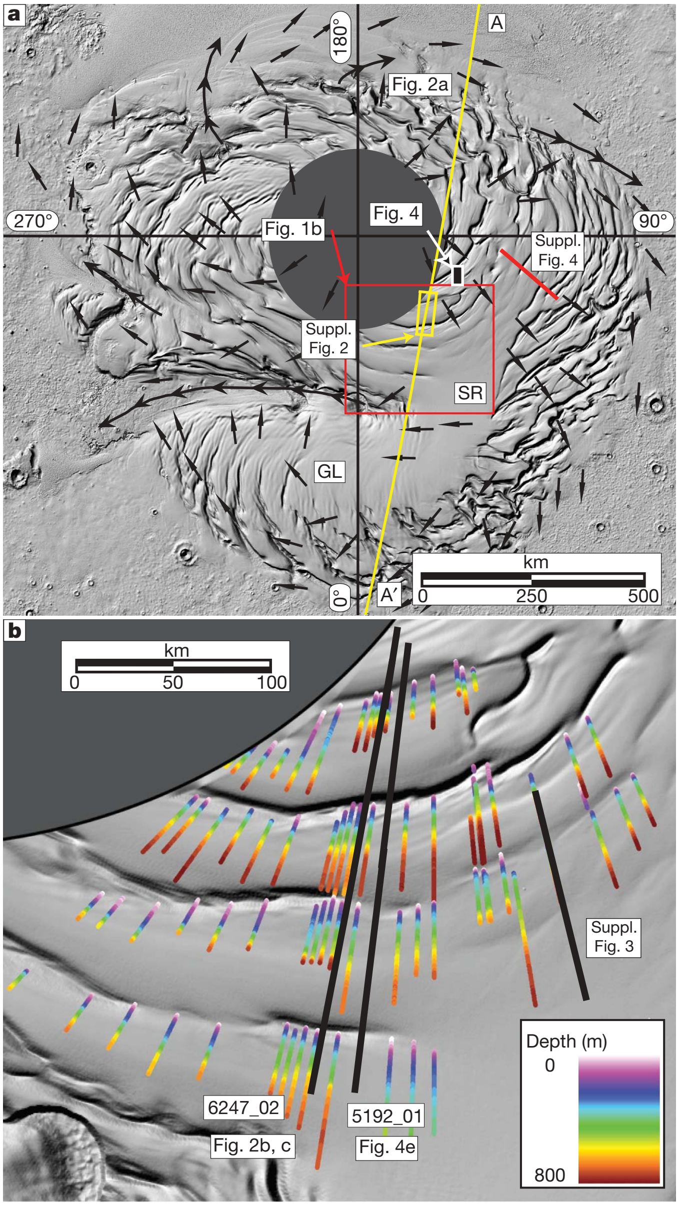

Figure 1 | NPLD with locations of data. **a**, Shaded-relief NPLD surface from MOLA elevation data[29] showing morphology of troughs, overall wind patterns from wind streak mapping[5] (black arrows) and locations of other figures. **b**, Upward projection of mapped discontinuities. Colours indicate trough migration path depth below surface. Location of orbit segments indicated in black. GL, Gemina Lingula; SR, saddle region.

[1]University of Texas Institute for Geophysics, Jackson School of Geosciences, Austin, Texas 78758, USA.

sheets on Earth since the 1970s, and more recently, two orbiting radars began collecting data at Mars: Mars Advanced Radar for Subsurface and Ionospheric Sounding (MARSIS)[21] on Mars Express and the SHAllow RADar (SHARAD) instrument[22] on the Mars Reconnaissance Orbiter. MARSIS was designed to probe deeply at the expense of resolution, while SHARAD, with a higher frequency and bandwidth (see Methods), has a vertical resolution of about 10 m in water ice and easily penetrates the ice-rich polar layered deposits[23,24] to reveal internal layering and structure[23]. Layers observed in radar (Fig. 2) are assumed to exhibit the same slopes and general structures as those in optical data, on the basis of gross comparisons in troughs (Fig. 2 and Supplementary Fig. 2), theoretical studies[25] and detailed correlations[26].

Below the spiral troughs, sloping discontinuities visible in SHARAD data interrupt sub-horizontal layering in the uppermost section[23] (Fig. 2). These discontinuities have slopes between 0.33 and 1.65 degrees, penetrate to between 500 and 700 m below the surface, and, in most cases, intersect the surface at a trough (Fig. 2b and c). The discontinuities are contiguous up to 65 km in length and always point down and to the south from the associated surface trough. In contrast, radar layers in the lower ~1,500 m of the NPLD are usually continuous for many hundreds of kilometres (Fig. 2a).

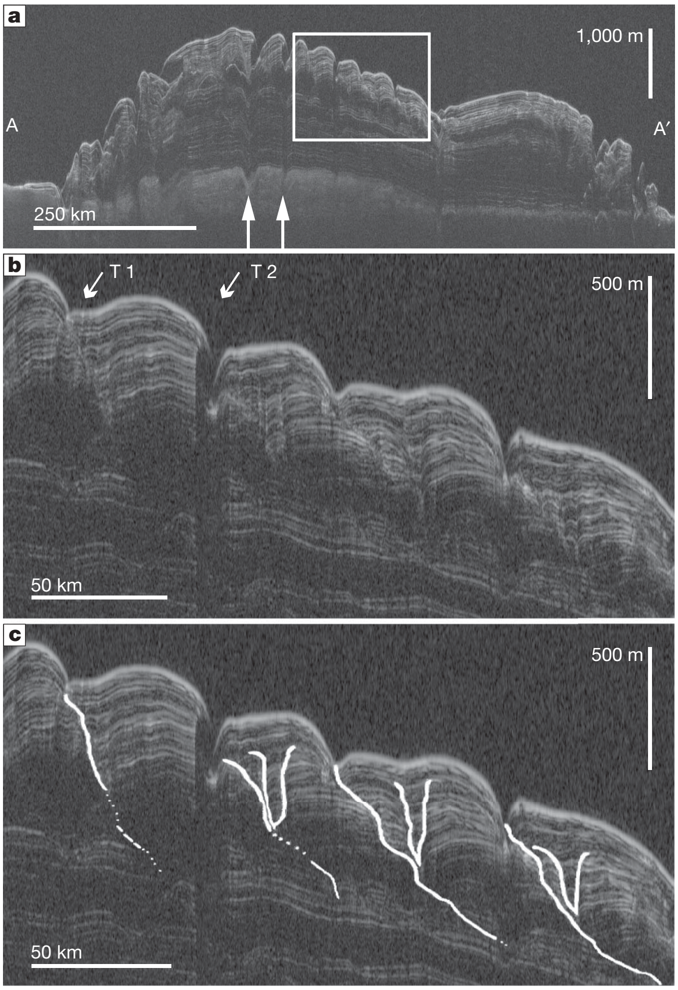

Figure 2 | SHARAD data over troughs. a, Observation 6247_02 (location indicated with yellow line in Fig. 1a), with vertical axis converted from time delay to depth assuming the dielectric constant of water ice. White arrows point to anomalies resulting from depth correction algorithm where MOLA topography is missing (for further discussion, see Supplementary Information). Vertical exaggeration is about 90:1. **b**, Expanded view of troughs (box in **a**) showing discontinuities and V-shaped structures in the upper 500 m. T1 and T2 (arrowed) are troughs 1 and 2, also shown in Supplementary Fig. 2. **c**, Same as Fig. 2b but with interpretation of data to delineate structures.

We examined troughs across the NPLD and in the south polar layered deposits (SPLD) to assess variability. The majority of NPLD troughs have discontinuities that can be traced below the surface to approximately 600 m (Figs 2 and 3e, and Supplementary Fig. 3) or 360 m in some cases (Supplementary Fig. 4). Because of regional accumulation variations[27], two discontinuities in the saddle region between Gemina Lingula and the main lobe (Fig. 1) extend farther below the NPLD surface but are at the same stratigraphic level as the 600-m discontinuities. Because they are steep and reach the substrate, troughs closer to the NPLD margin often have no associated stratigraphic record in radar to evaluate. Like the NPLD, the SPLD are deposited layers of water ice and dust of varying concentration, are more than 2 km thick, and have large spiral troughs covering the surface. In radar, however, the SPLD show few reflectors near the troughs, making it impossible to assess migration with this technique. Optical interpretations find no evidence of mass transport or trough migration in the south[7]. See Supplementary Information for examples and a discussion of SPLD trough stratigraphy.

Also observed, but more limited in number, are V-shaped structures (Fig. 2b and c) formed by a near-vertical alignment of inflections in downward bending layers. They are found adjacent to sloping discontinuities that reach a depth of 600 m, are contained within the uppermost ~400 m, and do not reach the surface. Undulations currently on the NPLD surface near 270° E and the western end of Gemina Lingula have topographic expressions that mimic these layers; see the orange horizons in Fig. 3e.

In map view, an overall pattern of the discontinuities following the spiral shape of the troughs becomes apparent (Fig. 1b). The less extensive V-shapes also follow this pattern. We interpret the spiralled, sloping discontinuities as positions through time of the south-facing scarps, or trough migration paths. In all cases the trough migration paths on the main lobe are deeper to the south, so the data support northward, upwind trough migration and a constructional origin of the troughs during deposition, as first hypothesized[2,3]. The troughs in Figs 2, 3, 4 and Supplementary Fig. 3 are about 65 km north of, and 620 m above, their initiation point (560 m of deposition and 60 m of upslope migration), although the exact depth varies depending on location. Other interpretations of the trough migration path as faults or as resulting from flow are not supported by the data. For a discussion of this and Earth analogues, see the Supplementary Information.

This new radar stratigraphy can be used to constrain the processes that have been proposed to govern trough migration[2–5]: solar ablation, wind transport, and atmospheric deposition. Any could be dominant under different climatic circumstances. First, uniform deposition adds a fresh layer of material to the polar layered deposits over an existing trough, raising the overall surface elevation. Katabatic winds descending into the trough approximately perpendicular to their length scour the equator-facing surface and remove material to be deposited downstream onto the pole-facing slope, causing both slopes to move northward[5] while thickening the downwind side (Fig. 3c). Such winds and their ability to move material have been observed (Fig. 4). In solar ablation, the slope most directly facing the Sun is warmed the most, causing preferential sublimation and retreat of that slope from the Sun[2] (Fig. 3b). Additional deposition forms new layers that drape the surface and are vertically offset across the trough.

The sum of these three processes gives rise to the trough migration path as a distinct feature that records the border between erosion and deposition, with its slope determined by the relative amounts of each. High deposition rates relative to erosion/transport increase the slope (less migration), while the opposite scenario decreases the slope (more migration). Thus the trough migration path slope indicates the relative balance between these climate-driven processes over time.

In a depositional regime accompanied by wind-dominated erosion and transport, layer thickness should depend on distance from the upwind scarp[2]. Layers will be uniform far from the trough but thinner along the upwind slope (cutting into lower layers if erosion

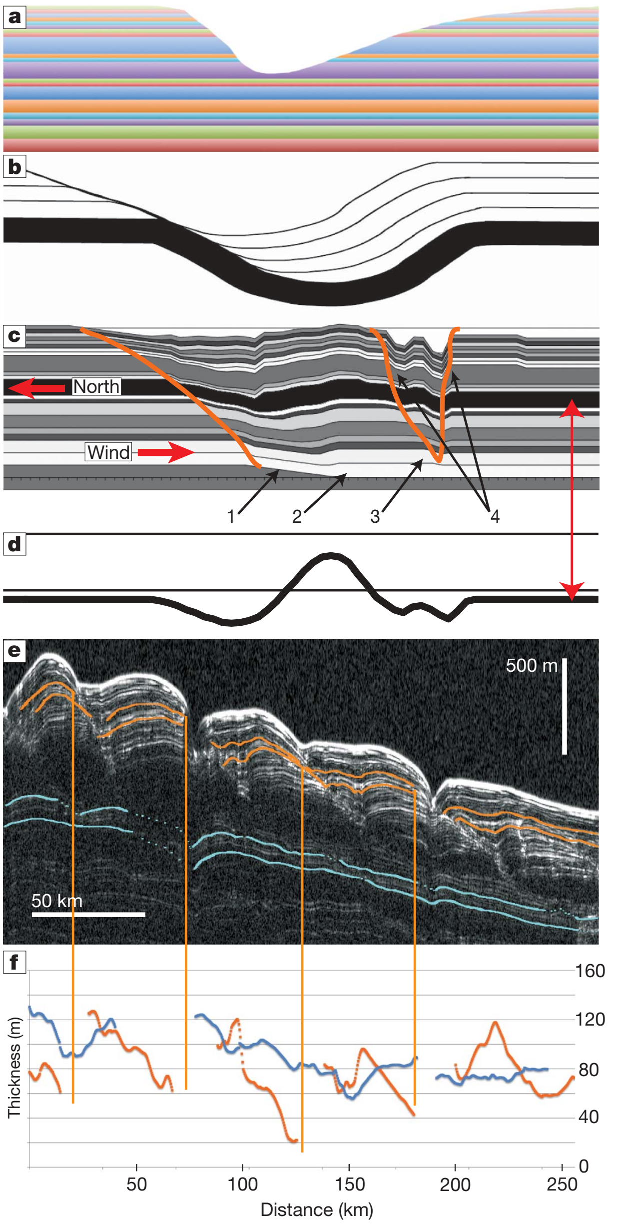

Figure 3 | Stratigraphy and layer thickness changes resulting from different proposed mechanisms of trough formation/migration. **a**, No trough migration. Layers are truncated by erosion but otherwise uniform in thickness and sub-horizontal. **b**, Trough migration caused by ablation of material on the equator-facing slope[2]. The trough migrates upward and northward, but layer thickness varies only on the south-facing slope. **c**, Wind-dominated stratigraphy. (1) Scouring on south-facing slope initiated at scarp. (2) Material transported southward assuming no material is lost to sublimation. (3) Small mound (or undulation) builds downwind, creating a secondary downwind face. (4) V-shape forms during subsequent deposition over the area between the leeward face of an undulation and farther downstream. **d**, Relative thickness of black layer in **c**, showing lateral change with respect to trough. **e**, SHARAD data from orbit 5192_01 (location indicated in Fig. 1b). Sub-horizontal layers (orange) are broken by sloping discontinuities and are vertically separated across the boundaries by approximately 150 m. Stratigraphic layers below the discontinuities (light blue) are more continuous and uniform in thickness. Vertical exaggeration is about 90:1. **f**, Plot of separation distance between reflector pairs shown in **e**. The change in thickness of the upper pair (orange) is similar to the pattern predicted by wind transport in **d**. For each trough, positions are indicated by vertical lines. Smaller variations in the lower layer (blue) may be related to regional deposition patterns or data processing algorithms.

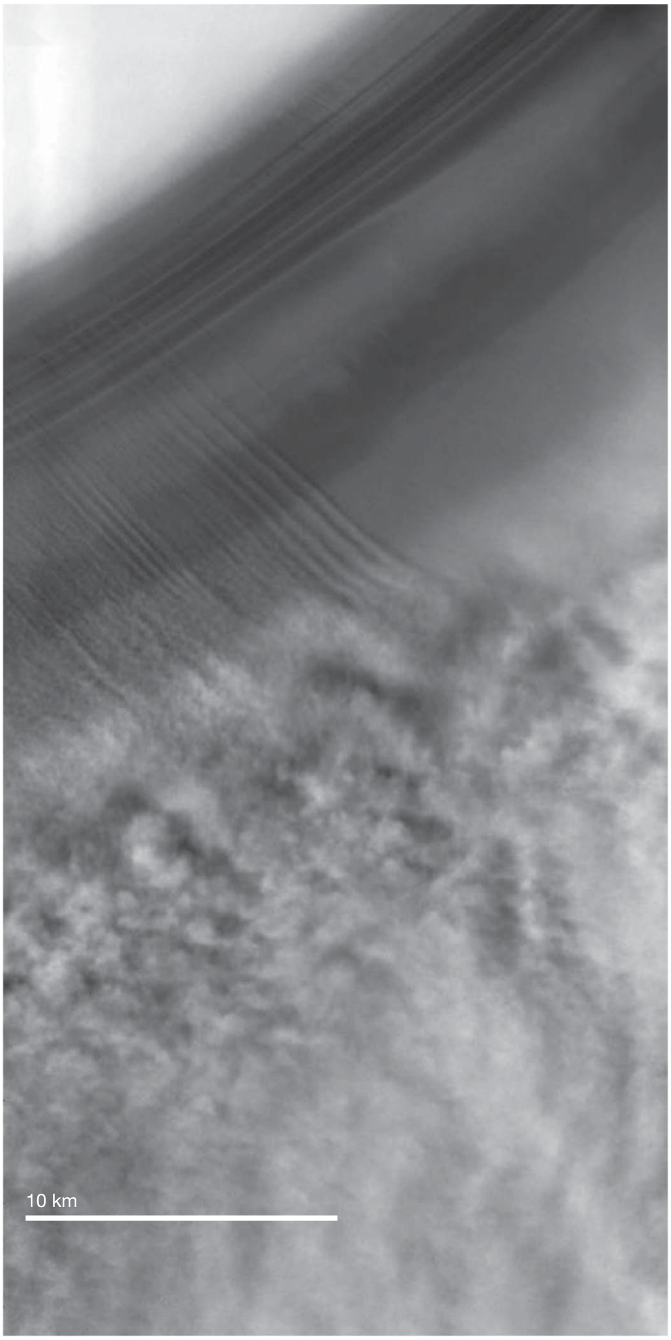

Figure 4 | Image of trough and effect of katabatic winds. Portion of THEMIS image V12432001 (ref. 30), showing laminar flow scouring the south-facing slope of a trough on the main lobe and moving material southward/downwind where it is then deposited. This image may be an uncommon example of extreme wind transport or a frequent, seldom observed occurrence. Location indicated in Fig. 1a.

exceeds deposition) and thicker on the downwind scarp[4]. Owing to this transport, a new local topographic high and associated slope may be created downwind that in turn can be eroded. This will result in undulations similar to those currently observed on the surface[1,2] (Figs 3c and d) and the V-shaped structures observed in the data (Fig. 2c). Stratigraphic thickness variations measured from radar layers across troughs (Fig. 3) are consistent with this scenario and hence with a dominant role for wind erosion and transport. Mapped wind patterns (Fig. 1a) are oriented roughly perpendicular to troughs, even where troughs are not aligned east–west.

Although solar ablation is plausible as the only cause of equator-facing slope retreat, layer thickness changes observed in the radar data do not match the uniform layer thicknesses predicted by solar ablation[2] (Figs 3c and d). However, we cannot rule out some component of solar ablation in slope retreat. Late-stage trough incision into the NPLD (for example, erosive downcutting by along-trough winds) is not supported by the radar data, because that would result in the truncation of layers on both sides of the trough (Fig. 3a), and equivalent layers would not be vertically offset.

A striking aspect of the radar data is that the stratigraphic layering representing older polar layered deposit surfaces is remarkably consistent from shortly after trough initiation until the present-day surface. Some instances in which layers on the equatorward slope were truncated (erosion/transport dominant) and then unconformably overlaid by a new layer that was preserved (deposition dominant) are observed (Figs 2 and 3), but the overall shape indicates that after initiation more than 560 m below the present surface, the processes governing trough morphology quickly reached a quasi-steady state that remained until the present or at least until very recently. Combining this with the evidence for a dominant role of wind in trough morphology and the mapped pattern of winds on the NPLD surface (Fig. 1a), it is likely that katabatic winds directed by the Coriolis force acted on the troughs from their initiation until now, having an important effect on their shape and position, including the spiral pattern.

Average accumulation rates in the NPLD are estimated to be between 0.28 and 1.2 mm yr^{-1} (ref. 28), and we use this to constrain trough age and migration rate. Using the 560–700-m trough initiation point, the main central troughs initiated between about 2.49 million years ago and 467,000 years ago and migrated on average 0.02–0.16 m yr^{-1}. The 360-m initiation point of troughs further east implies a younger age of between about 1.29 million years and 300,000 years. These ages do not account for possible depositional hiatuses. Higher deposition rates (that is, a younger age) might result in migration observable over decades, assuming the process is still active.

Before the troughs initiated, deposited layers were mostly continuous and uniform, indicating that different steady-state conditions prevailed then. What changes occurred in the Martian climate that suddenly created conditions favourable to trough formation is still unknown. With these new observations, perhaps climate models that include accumulation, solar ablation, feedback from regional and local topography, winds, and orbital forcing can better constrain these processes so that we can determine why the troughs began to appear on the NPLD only after three-quarters of its thickness was deposited.

METHODS SUMMARY

Theoretical[25] and empirical[26] studies indicate that radar reflections result from contrasts in the dielectric properties of visible NPLD layers and therefore serve to represent the same geometrical relationships. SHARAD data shown here were processed with a focused synthetic aperture radar technique to improve along-track resolution to about 300 m. Depth conversions assume a permittivity (real part) of 3.2, a value consistent with a composition of water ice at typical Mars temperatures. Layers and discontinuities are identified and mapped in time-delay data, before depth conversion, using Schlumberger's GeoFrame seismic interpretation software.

Received 16 December 2009; accepted 11 March 2010.

1. Cutts, J., Blasius, K. & Roberts, W. Evolution of Martian polar landscapes—interplay of long-term variations in perennial ice cover and dust storm intensity. *J. Geophys. Res.* **84,** 2975–2994 (1979).
2. Squyres, S. W. The evolution of dust deposits in the Martian north polar region. *Icarus* **40,** 244–261 (1979).
3. Howard, A. D. Origin of the stepped topography of the Martian poles. *Icarus* **34,** 581–599 (1978).
4. Howard, A. D., Cutts, J. A. & Blasius, K. R. Stratigraphic relationships within Martian polar cap deposits. *Icarus* **50,** 161–215 (1982).
5. Howard, A. D. The role of eolian processes in forming surface features of the Martian polar layered deposits. *Icarus* **144,** 267–288 (2000).
6. Tanaka, K. L. *et al.* North polar region of Mars: advances in stratigraphy, structure, and erosional modification. *Icarus* **196,** 318–358 (2008).
7. Kolb, E. J. & Tanaka, K. L. Geologic history of the polar regions of Mars based on Mars Global Surveyor data. II. Amazonian period. *Icarus* **154,** 22–39 (2001).
8. Milkovich, S. M. & Head, J. W. North polar cap of Mars: polar layered deposit characterization and identification of a fundamental climate signal. *J. Geophys. Res.* **110,** doi: 10.1029/2004JE002349 (2005).
9. Pelletier, J. D. How do spiral troughs form on Mars? *Geology* **32,** 365–367 (2004).
10. Winebrenner, D. P. *et al.* Evidence for ice flow prior to trough formation in the Martian north polar layered deposits. *Icarus* **195,** 90–105 (2008).
11. Head, J. W., Mustard, J. F., Kreslavsky, M. A., Milliken, R. E. & Marchant, D. R. Recent ice ages on Mars. *Nature* **426,** 797–802 (2003).
12. Fishbaugh, K. E. & Head, J. W. Origin and characteristics of the Mars north polar basal unit and implications for polar geologic history. *Icarus* **174,** 444–474 (2005).
13. Cutts, J. A. & Lewis, B. H. Models of climate cycles recorded in Martian polar layered deposits. *Icarus* **50,** 216–244 (1982).
14. Cutts, J. A. Wind erosion in the Martian polar region. *J. Geophys. Res.* 78 (20) 4211–4221 (1973).
15. Soderblom, L. A., Malin, M. C., Murray, B. & Cutts, J. Mariner 9 observations of the surface of Mars in the north polar region. *J. Geophys. Res.* **78,** 4197–4210 (1973).
16. Zeng, Z. *et al.* Evidence of fractures in NPLD and their significance to the formation of Martian polar spiral troughs. *39th Lunar Planet. Sci. Conf.* abstr. 2179 (Lunar and Planetary Institute, 2008) ⟨http://www.lpi.usra.edu/meetings/lpsc2008/pdf/2179.pdf⟩.
17. Ng, F. S. L. & Zuber, M. T. Patterning instability on the Mars polar ice caps. *J. Geophys. Res. Planets* **111,** E02005 (2006).
18. Fisher, D. A. Internal layers in an "accublation" ice cap: a test for flow. *Icarus* **144,** 289–294 (2000).
19. Weijermars, R. The polar spirals of Mars may be due to glacier surges deflected by Coriolis forces. *Earth Planet. Sci. Lett.* **76,** 227–240 (1986).
20. Fisher, D. A. If Martian ice caps flow: ablation mechanisms and appearance. *Icarus* **105,** 501–511 (1993).
21. Picardi, G. *et al.* Radar soundings of the subsurface of Mars. *Science* **310,** 1925–1928 (2005).
22. Seu, R. *et al.* SHARAD sounding radar on the Mars Reconnaissance Orbiter. *J. Geophys. Res. Planets* **112,** E05S05 (2007).
23. Phillips, R. J. *et al.* Mars north polar deposits: stratigraphy, age, and geodynamical response. *Science* **320,** 1182–1185 (2008).
24. Grima, C. *et al.* North polar deposits of Mars: extreme purity of the water ice. *Geophys. Res. Lett.* **36,** L03203 (2009).
25. Nunes, D. C. & Phillips, R. J. Radar subsurface mapping of the polar layered deposits on Mars. *J. Geophys. Res. Planets* **111,** E06S21 (2006).
26. Milkovich, S. M. & Plaut, J. J. Martian south polar layered deposit stratigraphy and implications for accumulation history. *J. Geophys. Res. Planets* **113,** E06007 (2008).
27. Holt, J. W. *et al.* The construction of Chasma Boreale on Mars. *Nature* doi:10.1038/nature09050 (this issue).
28. Fishbaugh, K. E. & Hvidberg, C. S. Martian north polar layered deposits stratigraphy: implications for accumulation rates and flow. *J. Geophys. Res. Planets* **111,** E06012 (2006).
29. Smith, D. E. *et al.* Mars Orbiter Laser Altimeter: experiment summary after the first year of global mapping of Mars. *J. Geophys. Res. Planets* **106,** doi: 10.1029/2000JE001364 (2001).
30. Christensen, P., Gorelick, N., Mehall, G. & Murray, K. THEMIS Public Data Releases. ⟨http://themis-data.asu.edu⟩ (Planetary Data System node, Arizona State University).

Supplementary Information is linked to the online version of the paper at www.nature.com/nature.

Acknowledgements This work was supported by NASA grant NAG5-12693 to J.H. and by the Gayle White Fellowship at the University of Texas Institute for Geophysics. We especially thank D. Young, S. Kempf, C. Brothers and S. Christian for listening to ideas and for help preparing the data and images. We thank A. Howard for insight and comments, and the SHARAD Operations Center for their continuous support in data acquisition. We dedicate this paper to the memory of SHARAD team member Ali Safaenili, who provided the focused radargrams we use. This is UTIG contribution 2187.

Author Contributions I.B.S. interpreted the data, created figures, and wrote the paper. J.W.H. wrote and edited the paper and figures and assisted in interpretation.

Author Information Data from the Mars Reconnaissance Orbiter, including SHARAD and HiRISE, are available at NASA's Planetary Data System (http://pds.jpl.nasa.gov/). Reprints and permissions information is available at www.nature.com/reprints. The authors declare no competing financial interests. Readers are welcome to comment on the online version of this article at www.nature.com/nature. Correspondence and requests for materials should be addressed to I.B.S. (isaac@ig.utexas.edu).

Contents:

S1) Clutter Simulations and Limitations of Depth Correction

While SHARAD can produce well-defined stratigraphy, data quality is influenced by acquisition geometry. In areas with large cross-track slopes, reflectors from surface topography to the sides (i.e. clutter) can arrive at the same time delay as reflectors from the subsurface directly below the spacecraft. Thus, the best geometry for observing stratigraphy beneath troughs occurs when the observation ground track is perpendicular to their orientation. Surface clutter reaches a maximum when the ground track runs parallel to the trough axes. The region between 0 and 90 degrees East longitude (Fig. 1) on the main NPLD lobe is well suited for this analysis due to the largely clutter-free geometry (Fig. S1).

Simulations created from elevation data show radar reflections that arise from the surface only and allow us to differentiate true subsurface reflectors from undesirable

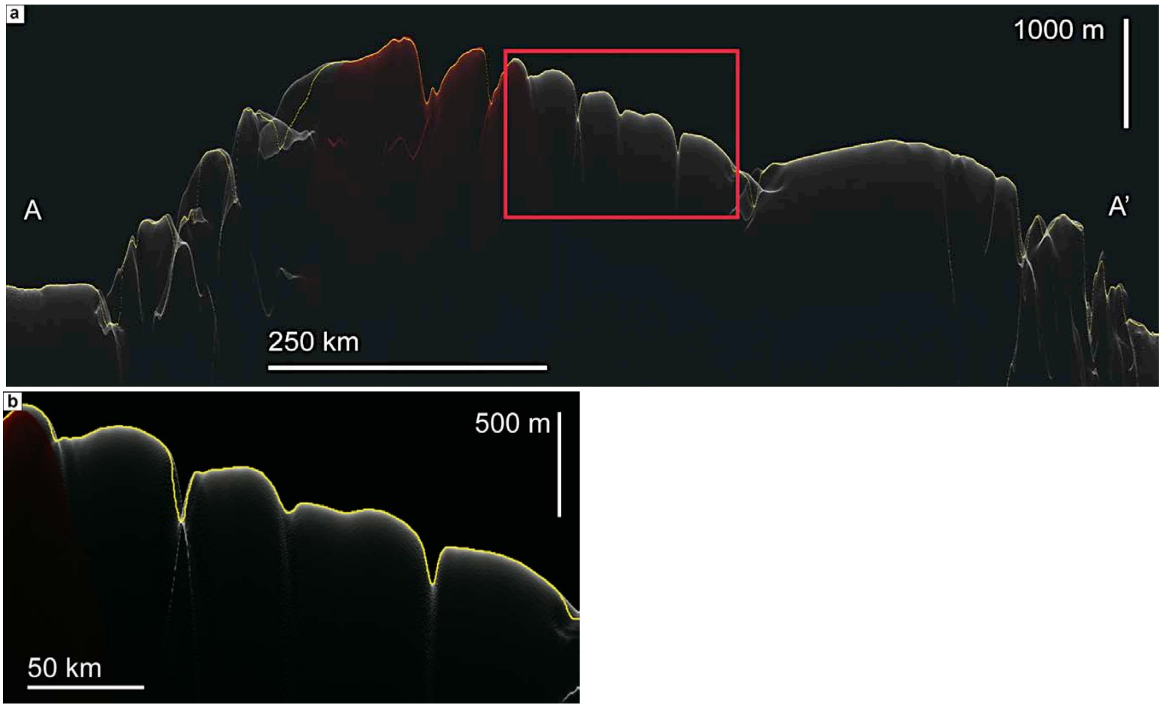

Figure S1. Simulated clutter for SHARAD observation 6247_02 (Fig 2). **a,** Profile covering the NPLD. NPLD margins are heavily cluttered, but area in red box has very little clutter. **b,** Detail within red box is shown in **a** and corresponds to Figs. 2b and 2c. Yellow line indicates MOLA elevation at nadir. Red zone within cluttergram indicates incomplete data due to MOLA coverage gaps at the pole.

clutter (Fig. S1). The clutter simulation was performed with a facet-based, incoherent scattering model[1] using spacecraft positioning and MOLA topography[2]. Furthermore, it is clear that the returns are from directly below the spacecraft, as indicated by the match between the first return and MOLA elevation at the nadir point in the simulation.

The depth correction algorithm aligns the radargram to the MOLA Digital Elevation Model and assumes that the surface reflection is from directly below the spacecraft, which is not the case always. Near the center of the NPLD (higher than

88°) there is very little elevation data, and what exists above 87.1° it is interpolated from sparse data. Because of the missing data, we are not able to correctly place the location of first reflection, which can be distant from the nadir point. Also, clutter simulations based on MOLA elevations will be inaccurate. This region is highlighted in red in Fig. S1.

S2) Comparison with Optical Data

Figure S2 shows imagery of two troughs with different surface expressions. SHARAD observations 6247_01 (Fig. 2b) and 5192_01 (Fig. 3e) both fall within this mosaic. The lower trough has steep slopes and exposed layers, while the upper is almost completely covered. This is manifested in radar data that show layers reaching the surface at the lower trough while the upper is covered (Fig. 2). Thus the gross morphology of radar layering agrees with that observed in imagery, and either deposition or local erosion may dominate in neighboring troughs.

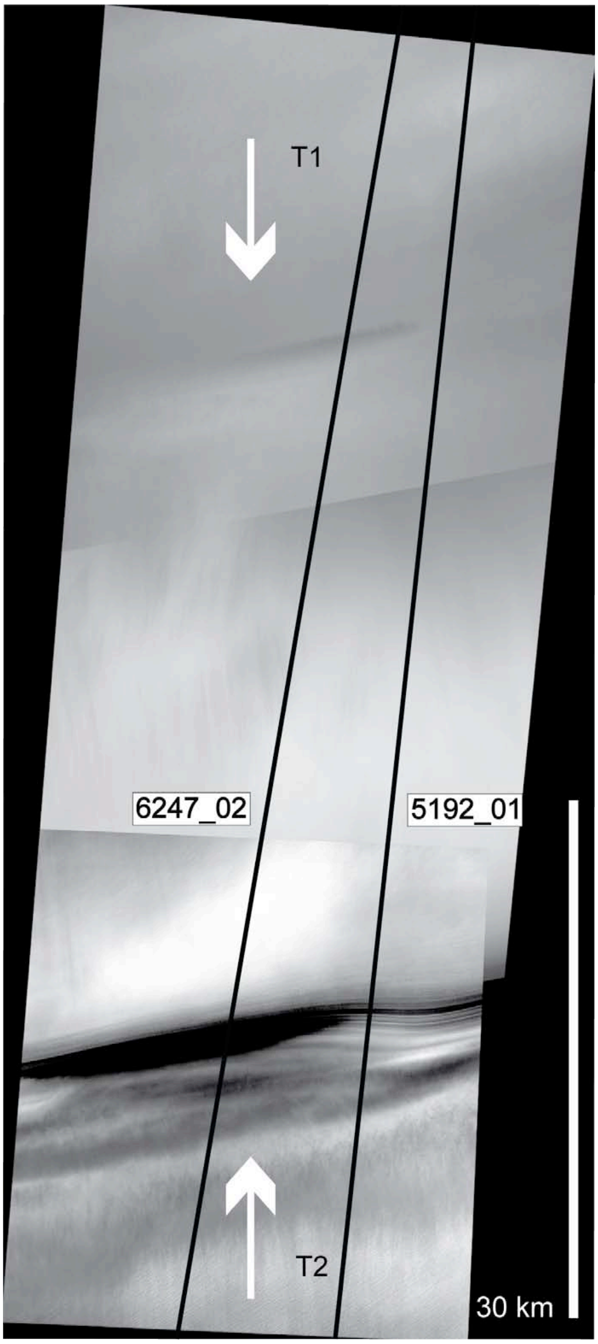

Figure S2. Surface expression of troughs from mosaic of Context Camera (CTX) images: P20_008755_2665, P20_009005_2655, P21_009 66_2729. Location of mosaic indicated in Fig. 1; T1 and T2 identified in Fig. 2. North is up in this mosaic.

S3) Terrestrial Analogs in Ice

In eastern Antarctica, large areas covered by dune-like features, termed megadunes, show radar reflector stratigraphy similar to that seen beneath the spiral troughs[3]. These megadunes have shorter amplitudes and wavelengths than the spiral troughs but share a characteristic upwind migration pattern. Additionally, the dune crests align themselves perpendicular to the prevailing katabatic wind, which maintain uniform direction and speed[4]. The dunes have long wavelengths and low amplitudes: 2 to 5 km and 2 to 4 m, respectively. This scales approximately 1:100 to the spiral troughs on the NPLD, which have ~50 km wavelengths and 320 to 400 m amplitudes for troughs shown in Fig 2.[5]. While these dimensions are much smaller, we feel that they are good for comparison. Megadunes in Wilkes Land, Antarctica, have estimated migration rates between 5 m and 25 m per year[3,6], two orders of magnitude greater than observed on Mars in this paper and from rates predicted in optical imagery[7]. Megadunes must form during times of relatively low accumulation and steady wind velocities to be so well organized. That is the case where they are found: in the middle of the ice sheet, far from passing storms[3]. A notable aspect of the megadunes is that they lie within regions where the slope is about 10 times that where dunes are not found: 0.10-0.15% vs. 0.013-0.022%[3]. This has been cited as an important control on megadune genesis[4], likely due to increased wind speed. So far, insolation is not linked to megadune formation. Wind transport, however, plays a very important role. The troughs on Mars may not have formed under the same conditions, but they have behaved similarly since initiation. Upwind migration, repeating patterns, perpendicular alignment to regional winds, and mass transport characterize both of these systems.

S4) Alternate Interpretations of Trough Stratigraphy

Faulting: Faulting of pre-existing layers would produce offset layers of equal thickness, a prediction unsupported by the radar data. Layering is also inconsistent with growth faults, as those would exhibit layers thickening uniformly toward the fault surface on the headwall, with maximum thickness at the scarp[8]. This is not seen in the NPLD, where accumulation appears to vary more based on surface slope. Furthermore, radar layers just below the discontinuities are not offset, restricting potential faulting to the upper several hundred meters (an impractical strain scenario for such a uniform composition). There is also no evidence for an accommodation zone or pressure ridge below any trough, some of which are 600 km from the NPLD margin. Another argument against the faulting argument is that TMP slopes in observation 6247_02 (Fig. 2c) and adjacent orbits range from 0.9 to 2.1 degrees and average ~1.2 degrees, values much too small to allow movement over 65 km. Steeper slopes, indicating less migration, are observed in the upper section of some observations 6167_01 (Fig. S3) and 7616_02 (Fig. S4), but in those section layers are continuous across the TMP, which does not evidence faulting. We find it unlikely that brittle deformation, in the form of faulting, can occur over slopes this shallow, with no accommodation, and over such a great distance.

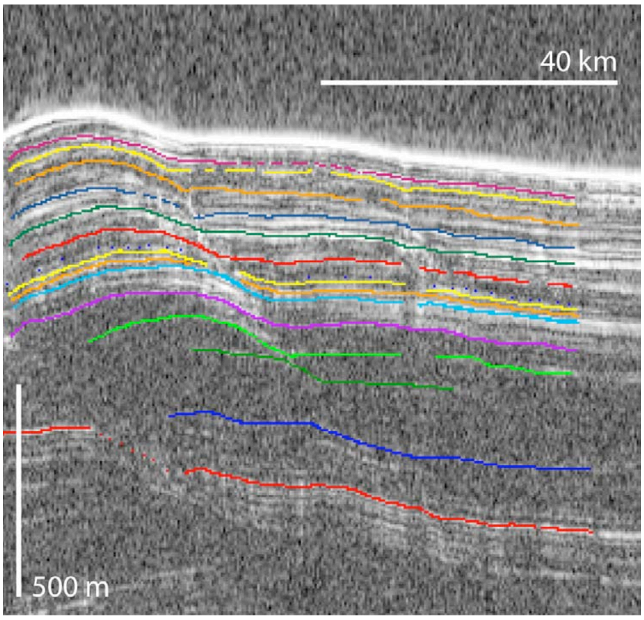

Figure S3. Segment of radargram 6167_01 (location indicated in Fig 1b). Stratigraphic reflectors traced across the TMP demonstrate continuity and lack of faulting.

Two further terrestrial examples with stratigraphic properties similar to the TMP including shallow slopes and layer offsets are found in the marine sediments of the Blake Ridge off the east coast of the United States[9] and the ‘Humboldt Slide’ near the Eel River in California[10]. Stratigraphic discontinuities in these sediments were

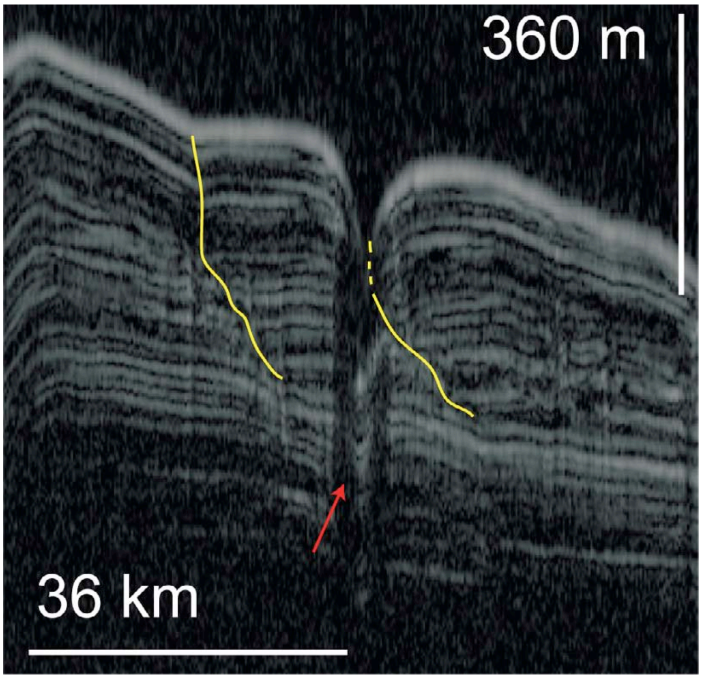

Figure S4. Segment of observation 7616_02 (location in Fig 1a). TMP, indicated by yellow lines, are seen beneath troughs as in Figure 2, but layer thickness does not vary as much as below other troughs. TMP begin about 360 m below the surface here. Artifact, indicated by red arrows, is the result of steep slopes on the surface of the PLD and the depth correction algorithm. A TMP slope change, seen best on the left, indicates a temporal change in the ratio of deposition to transport.

originally interpreted as submarine failures[11,12], but later, high-resolution seismic data as well as numerical and physical models revealed them to be large-scale sediment waves created by preferential erosion of upstream slopes combined with deposition[9,10]. Discussion about marine sediment waves versus faulting continues[8], however the data more strongly support the aggradational rather than the deformation hypothesis.

The radar data below many troughs on the NPLD show a strong correlation to the seismic data of sediment waves on Earth. In many cases (e.g. Fig. S3) internal reflectors can be traced across the inflection point (TMP) showing them to be continuous beds. Figure S3 crosses the same trough as Figures 2 and 3e (location in Fig. 1b) near enough to enable the connection of discreet reflectors but far enough that a different morphology (reflector continuity and lack of V-shape) is seen. Here we may eliminate faulting because the reflectors are continuous. They can then be extrapolated west towards 6247_02 and 5192_01. A differing ratio of processes (e.g., less wind relative to deposition) accounts for the morphology. Variations of insolation would make sense for the change in morphology if the troughs were at different latitudes, but Figure S3 contains the same trough as Figures 2 and 3e. It is, however, east of the other two observations, in a location of less regional slope. This indicates that the winds will accelerate less, pick up less material, and, therefore, cause less erosion. Furthermore, the slope of the TMP may be both concave up and concave down at different stratigraphic levels within the same radargram (Figures 2 and S3). This is the result of varying processes in a depositional regime and is not possible for normal faults, that only allow for linear or concave up discontinuities. Thrust faulting due to compression, allowing the concave down scenario, is unlikely given the stress regime which would result in outward deformation, if possible.

Flow: The geometry of layers seen in radar data does not match that predicted in models of flow[13], where layers bend upward below troughs due to less overburden. Instead, layers are sub-horizontal and of uniform thickness in the lower ~ 1500 m, and either conformal to the surface (i.e. downward bending) or truncated at troughs in the upper ~ 500 m. Modelling results compared to optical observations of layers over large distances indicate that flow has not occurred in the uppermost 500 m[14], consistent with the radar observations.

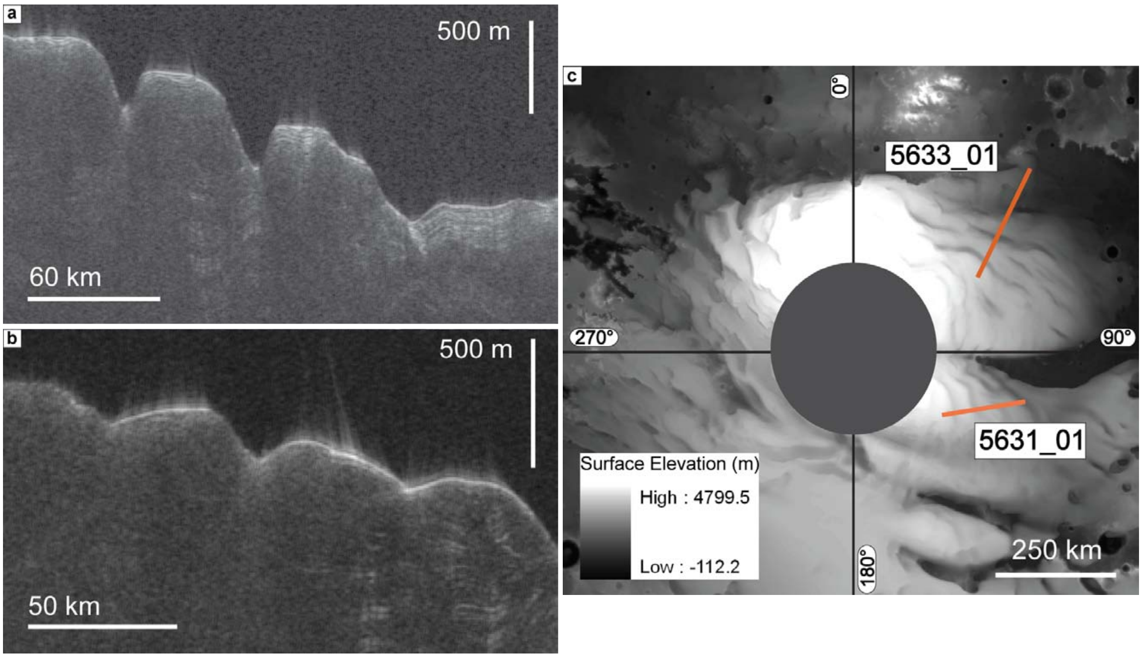

Figure S5. Radar observations of troughs on SPLD. a, Observation 5633_01. **b,** Observation 5631_01. Stratigraphic layers and discontinuities are not observed near troughs in the SPLD leaving no evidence for trough migration. **c.** Basemap showing locations of **a** and **b** on MOLA-derived surface. Gray circle indicates missing elevation data.

S5) Troughs of the South Polar Layered Deposits

SHARAD data in the SPLD show fewer layers relative to the NPLD, greatly limiting our technique there (Fig. S5). In general, there is a discrepancy between morphology of the NPLD and the south polar layered deposits (SPLD) in laser altimetry[2], optical, and radar data[15,16]. Some interpretations indicate that troughs in the south have not migrated and are late-stage erosional features[17]. Possible explanations for a different trough history in the SPLD include lower carrying capacity of wind due to the 6.4 km higher elevation and associated lower air density[18] and lack of deposition since approximately 5 Ma[18]. Additionally, unlike the NPLD, inter-trough undulations in the south are missing[19], supporting the interpretation of weaker winds and less material to move.

References for Supplementary Information

S1. Holt, J.W., Peters, M.E., Kempf, S.D., Morse, D.L. & Blankenship, D.D. Echo source discrimination in single-pass airborne radar sounding data from the Dry Valleys, Antarctica: Implications for orbital sounding of Mars. *Journal of Geophysical Research-Planets* **111**, E06S24 (2006).

S2. Smith, D.E. et al. Mars Orbiter Laser Altimeter: Experiment summary after the first year of global mapping of Mars. *Journal of Geophysical Research-Planets* **106**, 689-722, (2001).

S3. Frezzotti, M., Gandolfi, S. & Urbini, S. Snow megadunes in Antarctica: sedimentary structure and genesis. *Journal of Geophysical Research-Atmospheres* **107**, 4344 (2002).

S4. Fahnestock, M.A. et al. Snow megadune fields on the East Antarctic Plateau: extreme atmosphere-ice interaction. *Geophysical Research Letters* **27**, 3719–3722 (2000).

S5. Pathare, A.V. & Paige, D.A. The effects of martian orbital variations upon the sublimation and relaxation of north polar troughs and scarps. Icarus **174**, 419-443 (2005).

S6. Black, H.P. & Budd, W. Accumulation in the region of Wilkes, Wilkes Land, Antarctica. *Journal of Glaciology* **5**, 3-15 (1964).

S7. Howard, A.D., Cutts, J.A. & Blasius, K.R. Stratigraphic relationships within Martian polar cap deposits. Icarus **50**, 161-215 (1982).

S8. Nittrouer, C. *Continental Margin Sedimentation: From Sediment Transport to Sequence Stratigraphy*. (John Wiley & Sons, Ltd: Oxford, 2007).

S9. Holbrook, W.S. et al. Escape of methane gas through sediment waves in a large methane hydrate province. *Geology* **30**, 467–470 (2002).

S10. Lee, H.J. et al. Distinguishing sediment waves from slope failure deposits: field examples, including the 'Humboldt slide', and modelling results. *Marine geology* **192**, 79–104 (2002).

S11. Dillon, W.P. et al. Evidence for faulting related to dissociation of gas hydrate and release of methane off the southeastern United States. *Geological Society London Special Publications* **137**, 293 (1998).

S12. Lee, H., Edwards, B. & Field, M. Geotechnical analysis of a submarine slump, Eureka, California. *Offshore Technology Conference* (1981).

S13. Fisher, D.A. Internal Layers in an "Accublation" Ice Cap: A Test for Flow. *Icarus* **144**, 289-294 (2000).

S14. Fishbaugh, K.E. & Hvidberg, C.S. Martian north polar layered deposits stratigraphy: Implications for accumulation rates and flow. *Journal of Geophysical Research-Planets* **111**, E06012 (2006).

S15. Seu, R. et al. Accumulation and Erosion of Mars' South Polar Layered Deposits. *Science* **317**, 1715 (2007).

S16. Phillips, R.J. et al. Mars North Polar Deposits: Stratigraphy, Age, and Geodynamical Response. *Science* **320**, 1182 (2008).

S17. Kolb, E.J. & Tanaka, K.L. Geologic History of the Polar Regions of Mars Base on

Mars Global Surveyor Data II. Amazonian Period. *Icarus* **154**, 22-39 (2001).
S18. Herkenhoff, K.E. & Plaut, J.J. Surface ages and resurfacing rates of the polar layered deposits on Mars. *Icarus* **144**, 243-253 (2000).
S19. Howard, A.D. The Role of Eolian Processes in Forming Surface Features of the Martian Polar Layered Deposits. *Icarus* **144**, 267-288 (2000).